Journal of the European Ceramic Society 22 (2002) 1673–1681

www.elsevier.com/locate/jeurceramsoc

Evaluation of yttrium-doped $SrTiO_3$ as an anode for solid oxide fuel cells

Shiqiang Hui, Anthony Petric*

Department of Materials Science and Engineering, McMaster University, Hamilton, Ontario, Canada L8S 4L7

Received 14 June 2001; received in revised form 5 October 2001; accepted 28 October 2001

Abstract

Yttrium-doped $SrTiO_3$ (SYT) was assessed as an anode material for solid oxide fuel cells in terms of electrical conductivity, phase stability, redox behavior, chemical compatibility with yttria-stabilized zirconia (YSZ) and $La_{0.8}Sr_{0.2}Ga_{0.8}Mg_{0.2}O_{2.8}$ (LSGM), thermal expansion coefficient, and fuel cell performance. With the optimized composition $Sr_{0.86}Y_{0.08}TiO_{3-\delta}$, the electrical conductivity was as high as 82 S/cm at 800 °C and oxygen partial pressure of 10^{-19} atm. A reversible change of conductivity was observed upon oxidation and reduction. The resistance to oxidation was enhanced by partially replacing Ti with transition metals such as cobalt. This material has high structural stability over a broad range of temperature (up to 1400 °C) and oxygen partial pressure (1–10^{-20} atm). No phase change was found for mixtures of SYT with YSZ or LSGM sintered at 1400 °C for 10 h. The thermal expansion of doped-$SrTiO_3$ was determined to be compatible with that of YSZ and LSGM. A maximum power density of 58 mW/cm^2 at 900 °C was obtained for single cells with the new anode.

Keywords: Electrical conductivity; Fuel cells; Perovskites; (Sr,Y)TiO_3; Thermal expansion

1. Introduction

The goal to develop single phase mixed ionic and electronic conductors (MIEC) as anodes for solid oxide fuel cells (SOFC) is a continuing and elusive challenge. This type of anode material offers a number of advantages over the standard Ni–YSZ cermet anode.

First, in mixed conductors where both oxygen ions and electrons are mobile, the electrochemical reactions occur over the entire electrode/gas interfacial area. The usual requirements of a triple phase contact between electrode, electrolyte and gas, are replaced by a simple requirement of a two-phase boundary region between electrode and gas phase. The positive effect of mixed conductors at the interface has been well known for many years.[1–4] Thus, polarization losses with a mixed conducting electrode are expected to be significantly less than with electrodes exhibiting only electronic conductivity.[5–6]

Second, sulfur poisoning might not be so problematic because ceramics have a lower affinity for sulfur.

Finally, ceramic anodes have advantages in producing direct electrochemical oxidation of dry methane without carbon deposition. Steele et al. have demonstrated that platinum anodes are poor electrocatalysts for the oxidation of CH_4 at 800 °C.[7] However Bi_2O_3–Pr_6O_{11} anodes could electrochemically oxidize 100% CH_4 to CO_2 and H_2O at reasonable efficiencies without producing carbon deposition.[8]

CeO_2 based materials have been evaluated for SOFC anode applications.[9–11] Doped CeO_2 exhibiting mixed conduction in the fuel environment have been studied both as single phase materials and as two-phase mixtures with nickel. The CeO_2 anodes have shown considerable promise as electrode materials for direct oxidation of CH_4. However, anodes based on doped CeO_2 have not replaced nickel/YSZ anodes because of the relatively low levels of electronic conductivity and the relatively large lattice expansion associated with the loss of oxygen under anodic conditions, which can eventually result in the anode spilling off the electrolyte.[11]

Various oxides in addition to CeO_2 have also been investigated, including Y_2O_3–ZrO_2–TiO_2 solid solution, Mo-doped $Gd_2Ti_2O_7$, La-doped $SrTiO_3$, and a number of titanate systems such as $Mg_{1-y}Ti_{2+y}O_5$ and $Mg_{1-y}Ti_{1+y}O_3$.[12–15]

* Corresponding author. Tel.: +1-905-525-9140; fax: +1-905-528-9295.

E-mail address: petric@mcmaster.ca (A. Petric).

0955-2219/02/$ - see front matter
PII: S0955-2219(01)00485-X

So far, however, it has not been possible to develop a single phase material that is stable over the oxygen partial pressure range typically associated with anode operation and that exhibits sufficient electronic conductivity. Identifying anode materials that satisfy all requirements simultaneously is a significant challenge. Some of the required properties deteriorate when others are improved, as for example, electronic conductivity versus ionic conductivity or single-phase composition versus stability over a wide range of oxygen partial pressure. To optimize the anode materials requires a compromise in the chemical and physical properties.

We have recently measured unusually high electrical conductivity for yttrium-doped $SrTiO_3$ (SYT) under reducing atmospheres.[16] In this work, the chemical and physical properties of SYT were studied in terms of redox behavior, chemical compatibility with yttria-stabilized zirconia (YSZ) and $La_{0.8}Sr_{0.2}Ga_{0.8}Mg_{0.2}O_{2.8}$ (LSGM), thermal expansion coefficient (TEC), and fuel cell performance. Of all the systems investigated, the $Sr_{0.85}Y_{0.10}Ti_{0.95}Co_{0.05}O_{3-\delta}$ composition appears to be the most probable candidate for an SOFC anode.

2. Experimental

Doped $SrTiO_3$ specimens were synthesized by solid state reaction at high temperature as described in previous work.[17] The samples for four-point conductivity measurement were about 6 mm diameter by 15 mm long.

A gas mixture of carbon monoxide and carbon dioxide, controlled by an MKS mass-flow controller, type 1159B and an MKS readout, type 247C, was used to fix different oxygen partial pressures. The effective oxygen pressures depend on the ratio of CO and CO_2 according to the equilibrium:

$$CO_2 = CO + \frac{1}{2}O_2 \quad (1)$$

The effective range of control, which can be achieved at 800 °C, is 10^{-14}–10^{-20} atm of P_{O_2}.

The conductivity was measured by the standard four-probe dc method. The sample was placed in a holder, and external platinum leads were attached to both ends. A current of 0.1 A from a Keithley 225 current source was passed through the sample and the voltage drop was monitored by an HP 34401A multimeter. The input impedance of the multimeter was 10^{10} ohms. All the measurements were taken after the gas mixture had been allowed to equilibrate for at least one hour, and no significant change in conductivity was observed.

The fracture microstructures of yttrium-doped $SrTiO_3$, as prepared under reducing conditions, were examined with a Philips 515 scanning electron microscope. No coating was applied to the sample surface.

The oxygen vacancy concentration was determined by thermogravimetric analysis in a Netzsch STA 409 thermal balance under an atmosphere of flowing air at 1000 °C. The method is based on the weight change observed as a function of temperature or time. The error in the experimental weight gain is estimated to be ±0.05%.

An electrolyte disc (10 mm in diameter and 0.5 mm in thickness) was prepared by sintering pressed YSZ powder at 1400 °C for 10 h. A doped-$SrTiO_3$–glycol slurry was then painted on one side of the YSZ disc to make a half cell and annealed at 1200 °C in air for 2 h followed by a reduction of the anode at 1400 °C in 7% H_2 for 5 h. Pt paste (Engelhard) was applied on both sides of the cell as current collector and/or cathode. The active electrode area of the anode and cathode was 0.35 cm^2 each. The single cell was sealed to an alumina tube with Aremco cement. Gaseous H_2 saturated with water vapor at room temperature was supplied to the anode, and air was used as the oxidant at the cathode. A test cell schematic is shown in Fig. 1.

3. Results and discussion

3.1. Grain size of $Sr_{1-1.5x}Y_xTiO_{3-\delta}$ (SYT)

Fracture surfaces of $Sr_{1-1.5x}Y_xTiO_{3-\delta}$ ($x = 0.02$, 0.04, 0.06, 0.08) sintered at 1400 °C for either 10 or 20 h were examined by scanning electron microscopy as shown in Fig. 2. In all cases, the grain size varied only slightly from 3 to 6 μm. Grain growth in $SrTiO_3$ and $BaTiO_3$ have been reported to be highly sensitive to donor-doping.[18–20] At low donor concentrations, grain growth may become pronounced during high temperature sintering, often resulting in 50–100 μm grains, but at high donor concentrations grain growth is suppressed, with resulting grains of a few microns in size as were observed here. Burn and Neirman (1982)[18] found that the threshold in Y-doped $SrTiO_3$ was close to 1%, depending on the overall lattice cation stoichiometry. While this so-called donor-anomaly has been the subject of much research, to date a clear mechanistic interpretation has not been proposed.

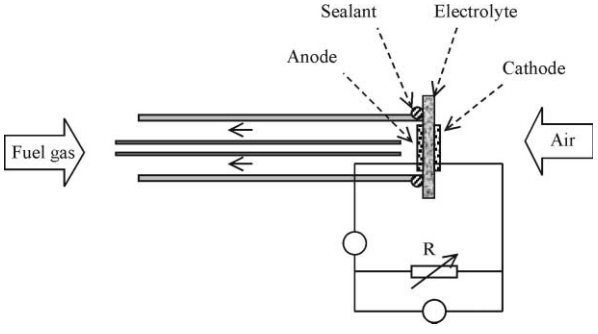

Fig. 1. Schematic of fuel cell test apparatus.

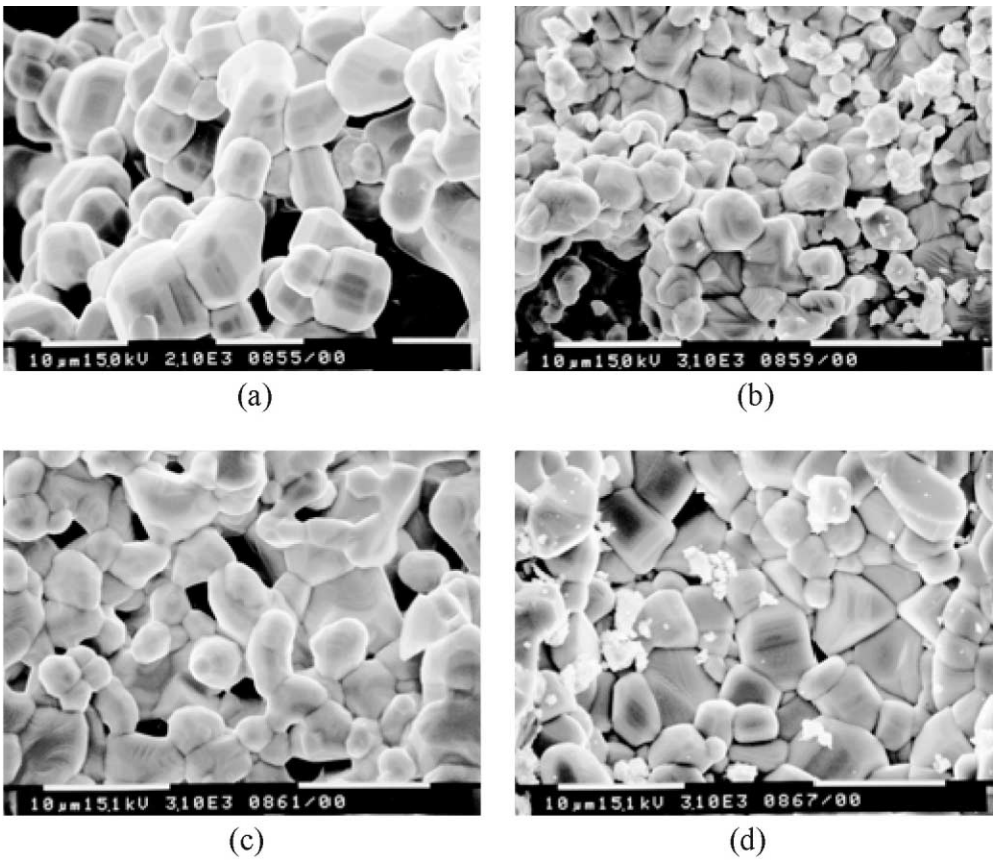

Fig. 2. SEM micrographs of fracture surfaces of Y-doped $SrTiO_3$ sintered at 1400 °C in air for various times: (a) $Sr_{0.97}Y_{0.02}TiO_{2.989}$ 10 h, (b) $Sr_{0.94}Y_{0.04}TiO_{2.980}$ 10 h, (c) $Sr_{0.91}Y_{0.06}TiO_{2.970}$ 10 h, (d) $Sr_{0.88}Y_{0.08}TiO_{2.968}$ 20 h.

Although the small grain structure may provide good mechanical properties, the accompanying large grain boundary area may impede electrical conductivity. Grain boundaries play an important role in the electrical properties of a variety of ceramic materials and components.

3.2. Redox behavior of $Sr_{0.88}Y_{0.08}TiO_{3-\delta}$

The rate of oxidation and reduction of $Sr_{0.88}Y_{0.08}TiO_{3-\delta}$ has been studied by measuring the change in the electrical conductivity as a function of time as the specimen was annealed in air and 7% H_2 (Fig. 3). The samples were initially reduced in forming gas at 1400 °C to obtain a reference conductivity under reducing conditions before the oxidation-reduction studies. The electrical conductivity changed rapidly with changing atmospheres either from forming gas to air (oxidation) or vice versa (reduction). One of the noticeable features is the parabolic time dependence of the change in electrical conductivity for both oxidation and reduction processes. Another observation is that conductivity was reversible on oxidation and reduction. However, the rate of reduction is much slower than that of oxidation, indicating that the incorporation of oxygen into lattice is much easier than the release of oxygen from lattice.

The oxidation-reduction reactions take place according to Eq. (2)

$$O_O \overset{\text{oxidation–reduction}}{\longleftrightarrow} 2e' + V_{\ddot{O}} + \frac{1}{2}O_2(g) \tag{2}$$

To be a useful material for fuel cell anodes, the change of electrical conductivity must be either rapid upon oxidation-reduction or kinetically hindered, especially for oxidation. The reduction of $Sr_{0.88}Y_{0.08}TiO_{3-\delta}$ involves the release of oxygen from the lattice, and results in the generation of electrons and oxygen vacancies. The opposite reaction occurs during the oxidation process. The extent of reduction or oxidation, η, is defined as

$$\eta = \frac{\Delta W_t - \Delta W_o}{\Delta W_\infty - \Delta W_o} \tag{3}$$

where ΔW is the weight loss, or oxygen deviation from stoichiometry, in relation to the stoichiometric composition, and t, o, and ∞ correspond to arbitrary time, initial state, and the final state, respectively.[21] Since the oxygen deviation is proportional to the electron concentration [Eq. (2)], one can express Eq. (3) in terms of conductivity as

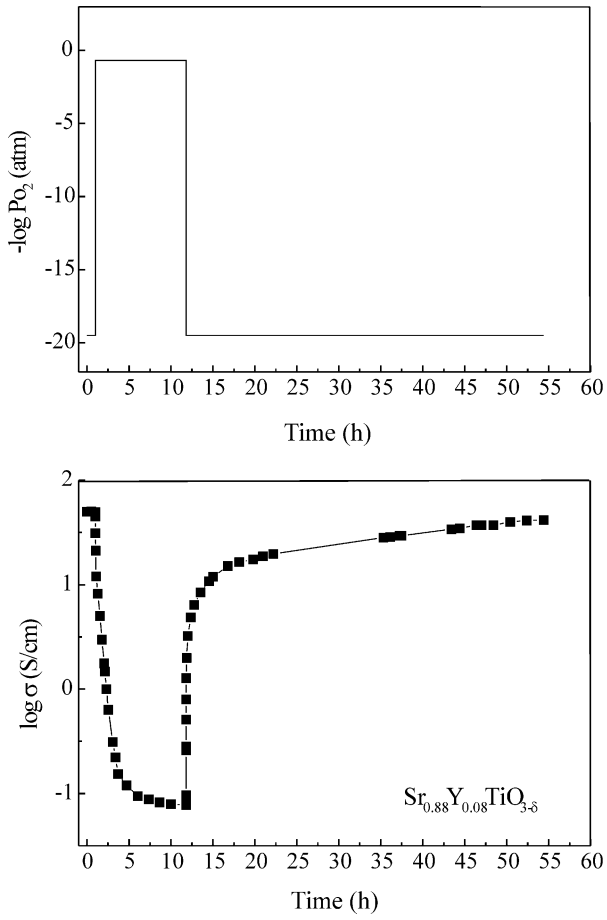

Fig. 3. Change of electrical conductivity for $Sr_{0.88}Y_{0.08}TiO_{3-\delta}$ at 800 °C after a sudden oxygen partial pressure change.

$$\eta = \frac{\sigma_t - \sigma_o}{\sigma_\infty - \sigma_o} \quad (4)$$

assuming the electron mobility is independent of concentration. As can be seen, the degree of reduction is a time dependent parameter.

Two processes in series have been proposed for the oxidation and reduction reactions, the gas-solid interface reaction and the bulk diffusion of relevant species, one of which is rate controlling.[22] As shown in Fig. 3, the conductivity of $Sr_{0.88}Y_{0.08}TiO_{3-\delta}$ changes rapidly at first, and reaches a plateau after some time. This behavior is typical for diffusion controlled processes, indicating a fast surface reaction at 800 °C for both oxidation and reduction. The composition changes must proceed by mass transport via diffusion from the gas–solid interface into the bulk (reduction) or from the bulk toward the gas–solid interface (oxidation). The kinetics of these oxidation–reduction processes depends therefore on the rate of diffusion or mobility of the oxygen vacancies. For the reduction process, the core of the $Sr_{0.88}Y_{0.08}TiO_{3-\delta}$ is reduced by diffusion of oxygen vacancies and reductant across the oxidized/reduced oxide interface whose area decreases with time. The distance of this interface from the surface of the specimen increases with time. Therefore, the rate of reduction or the conductivity decreases with time.

As pointed out elsewhere,[23] when temperature is changed, conductivity shows an effect due to the grain boundaries. For most oxides with a close-packed oxygen sublattice, oxygen diffusion at the grain boundaries appears to be rapid relative to diffusion within the grains. As a result, when oxygen partial pressure is changed, a stoichiometric change at the grain boundaries occurs preferentially.[24] The grain boundaries may act as fast conduction paths during reduction or as blocking layers during oxidation, via a conduction mechanism that is more or less independent of the grain properties.

3.3. Redox behavior of acceptor and donor Co-doped $SrTiO_3$

To evaluate the effects of acceptor addition at titanium-sites on the oxidation-reduction behavior, a number of samples with the composition $Sr_{0.85}Y_{0.10}Ti_{0.95}M_{0.05}O_{3-\delta}$ (M = V, Mn, Fe, Co, Ni, Cu, Ga, Al,) were studied by either electrical conductivity measurements or thermogravimetric analysis. The samples were equilibrated in 7% H_2 at 1400 °C for 10 h.

Fig. 4 shows the weight change for selected compositions during an oxidation-reduction cycle at a heating rate of 5 °C/min. The onset temperature, i.e., the lowest temperature for observed change of weight, the weight change, and the degree of reduction are summarized in Table 1. For all cases, the onset temperature for reduction is higher than that for oxidation, indicating a high activation energy for reduction. This is in accord with the relaxation time where the reduction process monitored by the conductivity took much longer than the oxidation process at the same temperature.

Because the oxidation and reduction is limited by oxygen vacancy diffusion through the oxide, and assuming diffusion occurs by the motion of isolated oxygen vacancies, any dopant that enhances the oxygen vacancy concentration should increase the oxidation and reduction rate. Correspondingly, the faster the oxygen diffusion is, the higher the degree of reduction for oxidized materials. The degree of reduction for $Sr_{0.85}Y_{0.10}Ti_{0.95}M_{0.05}O_{3-\delta}$ (M = Co, Cu, Ga, Al,) was indeed enhanced compared with that of $Sr_{0.85}Y_{0.10}TiO_{3-\delta}$. However, this was not observed for manganese or vanadium doped samples.

These results were consistent with the results of conductivity measurements. Fig. 5 shows the change of electrical conductivity during reduction in 7% H_2 at 800 °C for $Sr_{0.85}Y_{0.10}Ti_{0.95}M_{0.05}O_{3-\delta}$ (M = Mn, Co), along with the results for $Sr_{0.85}Y_{0.10}TiO_{3-\delta}$. Samples sintered in forming gas were equilibrated in air at 1400°C for 5 h before the conductivity measurement.

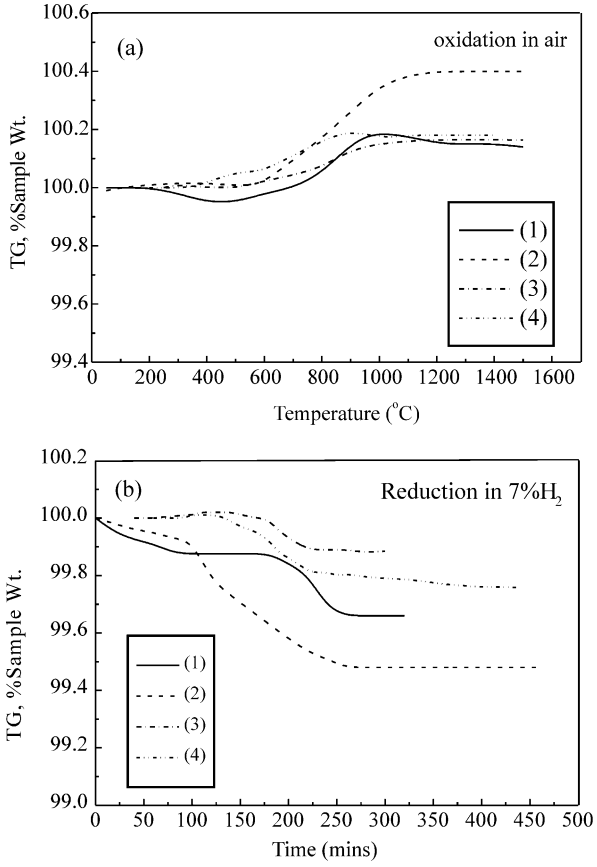

Fig. 4. Plots of thermogravimetric analysis during (a) oxidation process and (b) reduction process for (1) $Sr_{0.88}Y_{0.08}TiO_{3-\delta}$, (2) $Sr_{0.85}Y_{0.10}Ti_{0.95}Co_{0.05}O_{3-\delta}$, (3) $Sr_{0.85}Y_{0.10}Ti_{0.95}Ga_{0.05}O_{3-\delta}$, (4) $Sr_{0.85}Y_{0.10}Ti_{0.95}Cu_{0.05}O_{3-\delta}$.

The degree of reduction for $Sr_{0.85}Y_{0.10}TiO_{3-\delta}$, $Sr_{0.85}Y_{0.10}Ti_{0.95}Co_{0.05}O_{3-\delta}$ and $Sr_{0.85}Y_{0.10}Ti_{0.95}Mn_{0.05}O_{3-\delta}$ after a period of 24 h was 11.7, 17.3, and 2.1%, respectively. The addition of transition metals as donors in SYT not only enhanced the degree of reduction but also increased the resistance to oxidation.[17]

3.4. Effects of porosity

Porous anodes are used in fuel cells to allow gas access to the reaction sites without significant diffusion limitation. In order to evaluate the effect of porosity on conductivity, porous samples with compositions $Sr_{0.85}Y_{0.10}Ti_{0.95}Co_{0.05}O_{3-\delta}$ and $Sr_{0.88}Y_{0.08}TiO_{3-\delta}$ were made by adding 20 wt.% carbon black as a fugitive phase and annealing the samples in air at 1400 °C for 4 h. The relative density is estimated to be 72.8 and 69.5%, respectively.

Fig. 6 shows the change of conductivity of $Sr_{0.85}Y_{0.10}Ti_{0.95}Co_{0.05}O_{3-\delta}$ in the range of oxygen partial pressures of 10^{-14}–10^{-19} atm at 800 °C. A significant drop in conductivity was observed for the porous sample compared to the dense one. Juretscheke et al. have proposed a mathematical model to interpret the relationship of porosity and conductivity of ceramic materials.[25] Assuming that spherical pores are homogeneously distributed in dense materials, the relationship between relative conductivity and the porosity can be expressed as:

$$\sigma/\sigma^o = (1-\varepsilon)/(1+0.5\varepsilon) \quad (5)$$

Table 1
Results of thermogravimetric analysis (oxidation was carried out at a constant heating rate of 5 °C/min up to 1500 °C, reduction was carried out at 800 °C in 7% H_2 for 5 h)

Composition	Redox condition	Onset temperature (°C)	Weight change (%)	Degree of reduction (%)
$Sr_{0.88}Y_{0.08}TiO_{2.97}$	Oxidation	450	0.29	
	Reduction	900	0.19	66
$Sr_{0.85}Y_{0.1}Ti_{0.95}Co_{0.05}O_{3-\delta}$	Oxidation	550	0.40	
	Reduction	750	0.39	97
$Sr_{0.85}Y_{0.1}Ti_{0.95}Al_{0.05}O_{3-\delta}$	Oxidation	480	0.09	
	Reduction	850	0.09	100
$Sr_{0.85}Y_{0.1}Ti_{0.95}V_{0.05}O_{3-\delta}$	Oxidation	420	0.94	
	Reduction	550	0.52	55
$Sr_{0.85}Y_{0.1}Ti_{0.95}Cu_{0.05}O_{3-\delta}$	Oxidation	350	0.30	
	Reduction	670	0.30	100
$Sr_{0.85}Y_{0.1}Ti_{0.95}Ga_{0.05}O_{3-\delta}$	Oxidation	520	0.17	
	Reduction	720	0.16	94
$Sr_{0.85}Y_{0.1}Ti_{0.95}Mn_{0.05}O_{3-\delta}$	Oxidation	460	0.16	
	Reduction	620	0.06	38
$Sr_{0.85}Y_{0.1}Ti_{0.95}Ni_{0.05}O_{3-\delta}$	Oxidation	600	0.53	
	Reduction			
$Sr_{0.85}Y_{0.1}Ti_{0.95}Fe_{0.05}O_{3-\delta}$	Oxidation	550	0.39	
	Reduction			

where the porosity $\varepsilon = 1 - \rho/\rho^o$, ρ and ρ^o are the actual and theoretical density, respectively. The experimentally determined conductivity and porosity for $Sr_{0.85}Y_{0.10}Ti_{0.95}Co_{0.05}O_{3-\delta}$ are in accord with that predicted by Eq. (5).

Since the gas penetrates the materials via the pores so that diffusion lengths are greatly diminished, the oxidation and reduction rates are expected to be enhanced. This was confirmed by a comparison of conductivity change between dense porous and samples having composition $Sr_{0.88}Y_{0.08}TiO_{3-\delta}$ (Fig. 7). Typically, a rapid reduction was observed for the porous sample rather than the long period of reduction of the dense one, which is favored for the anode reduction in situ.

3.5. Compatibility with electrolytes

Since the SOFC membrane is a layered structure operating for long duration at elevated temperatures, chemical compatibility and thermal expansion compatibility of adjacent layers are essential.

Linear thermal expansion coefficients (TEC) of sintered samples (20 mm in length and 5 mm in diameter) were measured in air over the temperature range 25–1100 °C. Thermal expansion plots for several representative compositions are shown in Fig. 8, together with the thermal expansion of the electrolyte materials $Zr_{0.84}Y_{0.16}O_{1.92}$ and $La_{0.8}Sr_{0.2}Ga_{0.8}Mg_{0.2}O_{3-\delta}$ reported respectively by Männer et al. and Stevenson et al.[26,27] The TECs of various doped $SrTiO_3$ compositions remain constant with temperature and are near those of the electrolyte materials. Average TEC values for all the compositions are summarized in Table 2. Since the longitudinal thermal stress, σ_x, is a product of thermal expansion coefficient, α, and Young's modulus, E, as given by

$$\sigma_x = -\alpha TE \tag{6}$$

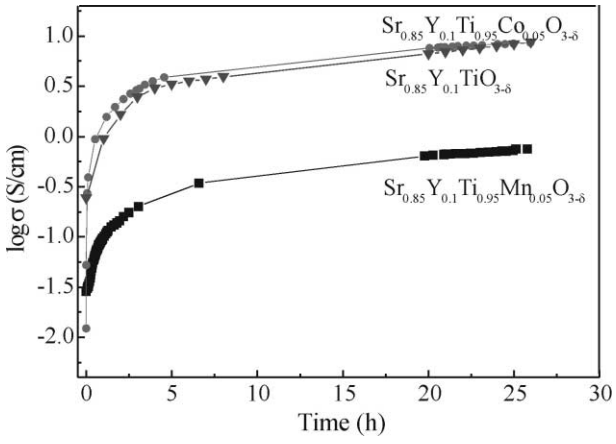

Fig. 5. Electrical conductivity as a function of time during reduction in 7% H_2 at 800 °C.

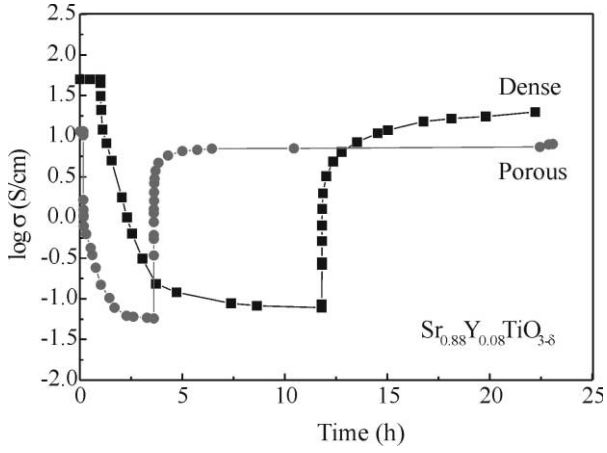

Fig. 7. Comparison of conductivity between dense and porous samples of $Sr_{0.88}Y_{0.08}TiO_{3-\delta}$ during oxidation–reduction processes at 800 °C.

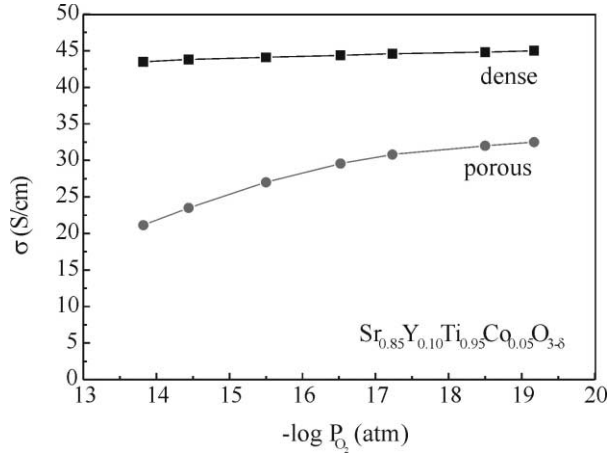

Fig. 6. Influence of porosity on electrical conductivity for $Sr_{0.85}Y_{0.10}Ti_{0.95}Co_{0.05}O_{3-\delta}$ at 800 °C.

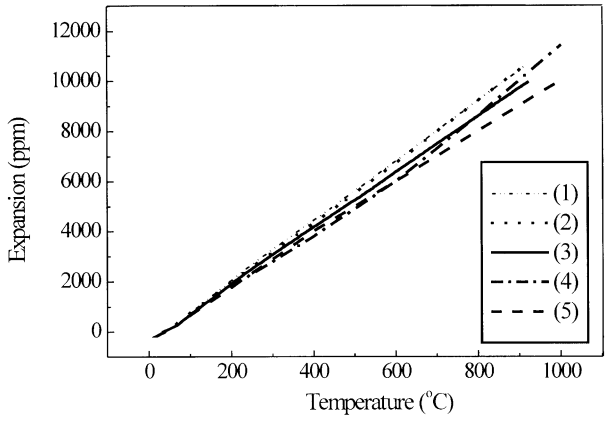

Fig. 8. Thermal expansion plots for (1) $Sr_{0.88}Y_{0.08}TiO_{3-\delta}$, (2) $Sr_{0.85}Y_{0.10}Ti_{0.95}Co_{0.05}O_{3-\delta}$, (3) $Sr_{0.85}Y_{0.10}Ti_{0.95}Al_{0.05}O_{3-\delta}$, (4) $La_{0.8}Sr_{0.2}Ga_{0.8}Mg_{0.2}O_{3-\delta}$, (5) $Zr_{0.84}Y_{0.16}O_{2-\delta}$.

where T is temperature, the difference of Young's modulus also has to be considered to avoid thermal stress failure.[28]

In order to assess the possible reactions of yttrium-doped $SrTiO_3$ with YSZ or LSGM at high temperatures, powder mixtures of $Sr_{0.88}Y_{0.08}TiO_{3-\delta}/Zr_{0.84}Y_{0.16}O_{2-\delta}$ (TZ-8Y, Tosoh Corp.) and $Sr_{0.88}Y_{0.08}TiO_{3-\delta}/La_{0.8}Sr_{0.2}Ga_{0.8}Mg_{0.2}O_{3-\delta}$ (Praxair) were pressed into pellets and sintered at 1400 °C for 10 h. Fig. 9 shows the XRD spectrum for the reacted samples. Peak overlaps were observed between $Sr_{0.88}Y_{0.08}TiO_{3-\delta}$ and $La_{0.8}Sr_{0.2}Ga_{0.8}Mg_{0.2}O_{3-\delta}$ because of the similar lattice parameters of the two oxides. No new phases were detected for either case under the experimental conditions. However, this examination could not determine the level of interfacial diffusion between the two phases and the resulting effects on conductivity. The addition of oxide impurities such as MgO, Ga_2O_3 and ZrO_2 which are components of the electrolytes, results in a decrease of the conductivity of $Sr_{0.85}Y_{0.10}TiO_{3-\delta}$ as shown in Fig. 10.

3.6. Fuel cell performance

Single cell tests were performed on electrolyte-supported cells with hydrogen and air. The electrolyte was 0.5 mm thick. The anode materials were applied as a paste and co-fired with the electrolyte. Pt paste was used for the cathode. Fig. 11 shows results of voltage (V) versus current density (J) measurements for SOFCs with anode composition (a) $Sr_{0.85}Y_{0.10}Ti_{0.95}Ga_{0.05}O_{3-\delta}$ and (b) $Sr_{0.85}Y_{0.10}Ti_{0.95}Co_{0.05}O_{3-\delta}$. Stable cell potentials

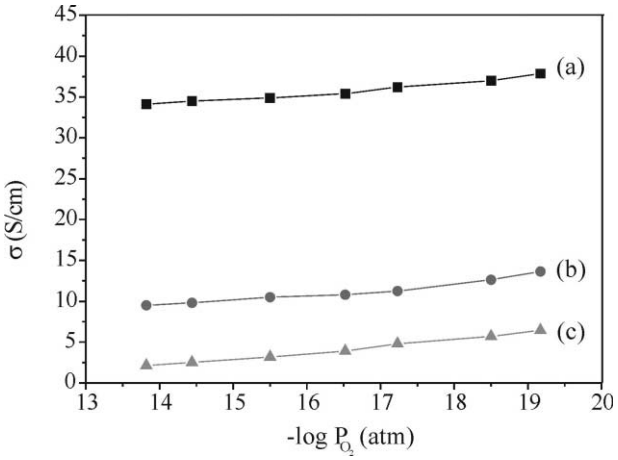

Fig. 10. Effect of 5% Ti substitution on the conductivity of $Sr_{0.85}Y_{0.10}TiO_{3-\delta}$ at 800 °C, by (a) Ga, (b) Zr, (c) Mg.

Table 2
Average thermal expansion coefficients of doped $SrTiO_3$ and electrolyte materials from 25 to 1100 °C

Composition	TEC ($\times 10^6$/°C)
$Sr_{0.88}Y_{0.08}TiO_{3-\delta}$	12.0
$Sr_{0.85}Y_{0.10}Ti_{0.95}Al_{0.05}O_{3-\delta}$	11.2
$Sr_{0.85}Y_{0.10}Ti_{0.95}Co_{0.05}O_{3-\delta}$	12.0
$Zr_{0.84}Y_{0.16}O_{1.92}$	10.8
$La_{0.8}Sr_{0.2}Ga_{0.8}Mg_{0.2}O_{3-\delta}$	11.3

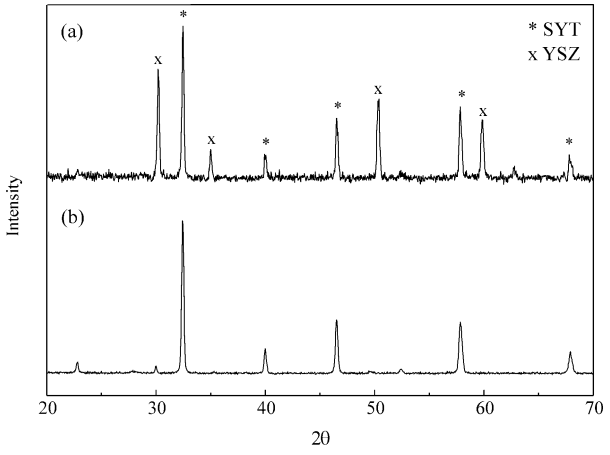

Fig. 9. X-ray spectrums for the sintered mixtures (a) $Sr_{0.88}Y_{0.08}TiO_{3-\delta} + Zr_{0.84}Y_{0.16}O_{2-\delta}$, (b) $Sr_{0.88}Y_{0.08}TiO_{3-\delta} + La_{0.8}Sr_{0.2}Ga_{0.8}Mg_{0.2}O_{3-\delta}$.

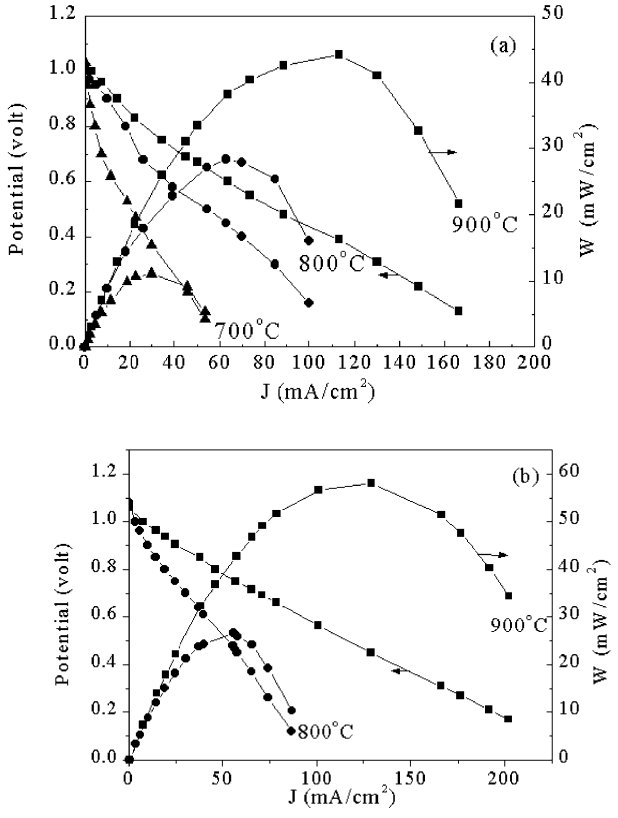

Fig. 11. Voltage and power density versus current for anodes with composition (a) $Sr_{0.85}Y_{0.10}Ti_{0.95}Ga_{0.05}O_{3-\delta}$, (b) $Sr_{0.85}Y_{0.10}Ti_{0.95}Co_{0.05}O_{3-\delta}$.

with a slight degradation were observed for a period of 24 h. Both current density and maximum power density increased with increasing temperature of operation. The cells with doped $SrTiO_3$ as anodes gave poor power density (max. 58 mW/cm^2 at 900 °C) although the standard open circuit potential was observed. Partial delamination of the anode was evident after cooling.

The efficiency of an SOFC depends mainly on its ohmic resistance and electrode polarization but can be minimized by material modification and cell fabrication. The resistance of the total cell was observed to be 780–1000 Ω at operating temperatures, which is much higher than that expected from the anode and the electrolyte. Upon examination of the ceramic membrane after the fuel cell tests, it was observed that the anode coating had separated from electrolyte. The poor power density observed in this study could be due to the high contact resistance between anode and electrolyte. If this is the case, the electrochemical performance of doped $SrTiO_3$ as the anode of the fuel cell was not well characterized. The ohmic resistance could be reduced by decreasing the thickness of electrolyte and electrodes, as has been demonstrated by lamination of slip-cast tapes and screen printed or sprayed electrodes.[29,30] Those researchers reported a power density up to 900 mW/cm^2 at 800 °C. Reducing the resistance to less than 10 Ω by decreasing the thickness of the membrane and improving interface contact is expected to improve the performance to industrial standards.

4. Conclusions

The conductivity of $Sr_{0.88}Y_{0.08}TiO_{3-\delta}$ is reversibly recovered from oxidized samples by reduction at 800 °C. However, the reduction rate is about four times slower than the oxidation rate. Thermogravimetric studies indicate that the reduction process starts at a higher temperature than the oxidation. Of the 5 mol% acceptor-doped compositions, the system $Sr_{0.85}Y_{0.10}Ti_{0.95}Co_{0.05}O_{3-\delta}$ had the highest conductivity of 45 S/cm at 800 °C and oxygen partial pressure of 10^{-19} atm, which dropped to 33 S/cm for a sample with 30% porosity.

No phase change was observed for mixtures of $Sr_{0.88}Y_{0.08}TiO_{3-\delta}$ with YSZ or LSGM fired at 1400 °C for 10 h. This suggests chemical compatibility between the yttrium-doped $SrTiO_3$ and the electrolytes. However, the effects of interfacial diffusion on conductivity have not been assessed. The thermal expansion coefficients (TEC) of doped-$SrTiO_3$ were determined to be compatible with those of YSZ and LSGM. SEM examination showed that the average grain size of $Sr_{1-1.5x}Y_xTiO_{3-\delta}$ ($0.02 \leqslant x \leqslant 0.08$) is 3–6 μm. The small grain size may provide good mechanical properties when SYT is used as the support structure in SOFC membranes.

Acknowledgements

This work was funded by the Natural Sciences and Engineering Research Council of Canada through Strategic Project STP 0201896 and by Global Thermoelectric Inc.

References

1. Inoue, T., Setoguchi, T., Eguchi, K. and Arai, H., *Solid State Ionics*, 1989, **35**, 285–291.
2. Eguchi, K., Setoguchi, T., Okamoto, K. and Arai, H., In *Proceedings of the 3rd International Symposium on SOFCs*, ed. S. C. Singhal and H. Iwahara. Electrochem. Soc., Pennington, NJ, 1993, pp. 494–503.
3. Setoguchi, T., Okamoto, K., Eguchi, K. and Arai, H., *J. Electrochem. Soc.*, 1992, **139**, 2875–2880.
4. Schäfer, W., Koch, A., Herold-Schmidt, U. and Stolten, D., *Solid State Ionics*, 1996, **86–88**, 1235–1239.
5. Schouler, E. J. L., *Solid State Ionics*, 1982, **9&10**, 945–952.
6. Liou, S. S. and Worrell, W. L., *J. Appl. Physics A*, 1989, **49**, 25–31.
7. Steele, B. C. H., Kelly, I., Middleton, H. and Rudkin, R., *Solid State Ionics*, 1988, **28-30**, 1547–1552.
8. Mogensen, M., In *Proceedings of the 2nd International Symposium on SOFCs*, ed. F. Groz, P. Zegers, S. C. Singhal and O. Yamamoto. Commission of the European Communities, Luxembourg, 1991, p. 577.
9. Metcalfe, I. S., Middleton, P. H., Petrolekas, P. and Steel, B. C. H., *Solid State Ionics*, 1992, **57**, 259–264.
10. Mogensen, M. and Bentzen, J. J., In *Proceedings of the 1st International Symposium SOFC*, ed. S. C. Singhal. Electrochem. Soc., Pennington, NJ, 1989, p. 99.
11. Mogensen, M., Lindegaard, T. and Hansen, U. R., *J. Electrochem. Soc.*, 1994, **141**, 2122–2128.
12. Worrell, W., *Solid State Ionics*, 1992, **52**, 147–151.
13. Porat, O., Heremans, C. and Tuller, H. L., *Solid State Ionics*, 1997, **94**, 75–83.
14. Slater, P. R., Fagg, D. P. and Irvine, J. T., *J. Mater. Chem.*, 1997, **7**(12), 2495–2498.
15. Fagg, D. P., Fray, S. M. and Irvine, J. T., *Solid State Ionics*, 1994, **72**, 235–239.
16. Hui, S. and Petric, A., *J. Electrochem. Soc.*, in press.
17. Hui, S. and Petric, A., *J. Mater. Chem.*, submitted.
18. Burn, I. and Neirman, S., *J. Mater. Sci.*, 1982, **17**, 3510–3524.
19. Yan, M. F., *Mater. Sci. Eng.*, 1981, **48**, 53–72.
20. Kahn, M., *J. Am. Ceram. Soc.*, 1971, **54**, 452–457.
21. Smyth, D. M., Advances in ceramics. In *Proc. Supercond. Symp.*, The Am. Ceram. Soc., Westerville, OH, 1989, pp. 99–103.
22. Philibert, J., *Solid State Ionics*, 1999, **117**, 7–11.
23. Hui, S., *Evaluation of Yttrium-doped $SrTiO_3$ as a Solid Oxide Fuel Cell Anode*. PhD thesis, McMaster University, Hamilton, 2000.
24. Kingery, W. D., *J. Am. Ceram. Soc.*, 1974, **57**, 1–8.
25. Juretscheke, H. J., Landauer, R. and Swanson, J. A., *J. Appl. Phys.*, 1956, **27**, 838–839.
26. Männer, R., Ivers-Tiffée, E. and Wersing, W., In *Proceedings of the 2nd International Symposium on SOFCs*, 1991, Athens, Greece, ed. F. Groz, P. Zegers, S. C. Singhal and O. Yamamoto. Commission of the European Communities, Luxembourg, 1991, p. 715.
27. Stevenson, J. W., Armstrong, T. R., McCready, D. E., Pederson, L. R. and Weber, W. J., *J. Electrochem. Soc.*, 1997, **144**, 3613–3624.
28. Timoshenko, S. and Goodier, J. N., *Theory of Elasticity*, 3rd edn. McGraw-Hill, New York, 1970 pp. 433–438.

29. Wang, C., Worrell, W. L., Park, S., Vohs, J. M. and Gorte, R. J., In *Proceedings of the 6th International Symposium on SOFCs*, 1999, Honolulu, HI, ed. S. C. Singhal and M. Dokiya, M., Electrochem. Soc., Pennington, NJ, 1999, pp. 851–860.

30. Primdahl, S., Jorgensen, M. J., Bagger, C. and Kindl, B., in *Proceedings of the 6th International Symposium on SOFCs*, 1999, Honolulu, HI, eds. S. C. Singhal and M. Dokiya. Electrochem. Soc., Pennington, NJ, 1999, pp. 793–802.